1-1-2005

Characterization of the Active Site and Insight into the Binding Mode of the Anti-angiogenesis Agent Fumagillin to the Manganese(II)-Loaded Methionyl Aminopeptidase from *Escherichia coli*

Ventris M. D'Souza
Utah State University

Robert S. Brown
Utah State University

Brian Bennett
Marquette University, brian.bennett@marquette.edu

Richard C. Holz
Marquette University, richard.holz@marquette.edu

Accepted version. *Journal of Biological Inorganic Chemistry*, Vol. 10, No. 1 (January 2005): 41-50.

Journal of Biological Inorganic Chemistry, Vol. 10, No. 1 (January, 2005). DOI.

Characterization of the Active Site And Insight Into the Binding Mode of the Anti-Angiogenesis Agent Fumagillin to the Manganese(II)-Loaded Methionyl Aminopeptidase from *Escherichia coli*

Ventris M. D'souza
Department of Chemistry and Biochemistry, Utah State University, Logan, UT
Robert S. Brown
Department of Chemistry and Biochemistry, Utah State University, Logan, UT
Brian Bennett
Department of Biophysics, The Medical College of Wisconsin, Milwaukee, WI
Richard C. Holz
Department of Chemistry and Biochemistry, Utah State University, Logan, UT

Abstract

EPR spectra were recorded for methionine aminopeptidase from *Escherichia coli* (*Ec*MetAP-I) samples (~2.5 mM) to which one and two equivalents of Mn(II) were added (the latter is referred to as [MnMn(*Ec*MetAP-I)]). The spectra for each sample were indistinguishable except that the spectrum of [MnMn(*Ec*MetAP-I)] was twice as intense. The EPR spectrum of [MnMn(*Ec*MetAP-I)] exhibited the characteristic six-line $g \approx 2$ EPR signal of mononuclear Mn(II) with $A_{av}(^{55}Mn)=9.3$ mT (93 G) and exhibited Curie-law temperature dependence. This signal is typical of Mn(II) in a ligand sphere comprising oxygen and/or nitrogen atoms. Other features in the spectrum were observed only as the temperature was raised from that of liquid helium. The temperature dependences of these features are consistent with their assignment to excited state transitions in the $S=1, 2 \ldots 5$ non-Kramer's doublets, due to two antiferromagnetically coupled Mn(II) ions with an $S=0$ ground state. This assignment is supported by the observation of a characteristic 4.5 mT hyperfine pattern, and by the presence of signals in the parallel mode consistent with a non-Kramers' spin ladder. Upon the addition of the anti-angiogenesis agent fumagillin to [MnMn(*Ec*MetAP-I)], very small changes were observed in the EPR spectrum. MALDI-TOF mass spectrometry indicated that fumagillin was, however, covalently coordinated to *Ec*MetAP-I. Therefore, the inhibitory action of this anti-angiogenesis agent on *Ec*MetAP-I appears to involve covalent binding to a polypeptide component at or near the active site rather than direct binding to the metal ions.

Keywords

Cobalt; Fumagillin; Manganese; Methionyl aminopeptidase; Peptide hydrolysis

Introduction

Methionyl aminopeptidases (MetAPs) represent a unique class of protease that is capable of the hydrolytic removal of an N-terminal methionine residue from nascent polypeptide chains.[1,2,3,4] In both eukaryotic and prokaryotic cells, MetAPs selectively cleave methionine residues from the N-termini of polypeptide chains. In the cytosol of eukaryotes, all proteins are initiated with an N-terminal methionine residue, whereas in prokaryotes, mitochondria, and chloroplasts, translation of proteins is initiated with an N-formyl methionine.[2,5,6,7] The N-formyl group is typically removed cotranslationally by a deformylase that leaves the N-terminal methionine with a free NH_2 group.[8] Removal of methionine is essential for protein maturation as well as for the post-translational modification of the N-termini of proteins, such as N-acetylation or N-myristoylation. Deletion of the gene encoding MetAP is lethal to*Escherichia coli*, *Salmonella typhimurium*, and *Saccharomyces cerevisiae*; therefore, MetAPs are essential for cell growth and proliferation.[9,10,11,12] The importance of understanding the catalytic mechanism of MetAPs is underscored by the recent observation that MetAPs are the target for anti-cancer drugs, one of which is in the third stage clinical trials.[13] Thus, the design of mechanism-based inhibitors is critically important in the development of drugs that prevent tumor growth and proliferation.

MetAPs are organized into two classes (types I and II) based on the absence or presence of an extra 62 amino acid sequence (of unknown function) inserted near the catalytic domain. The type-I MetAPs from *E. coli* (*Ec*MetAP-I) and *Staphylococcus aureus* (*Sa*MetAP-I) and the type-II MetAPs from *Homo sapiens* (*Hs*MetAP-II) and *Pyrococcus furiosus* (*Pf*MetAP-II) have been crystallographically

characterized.[14,15,16,17,18] All display a novel “pita-bread” fold with an internal pseudo-two-fold symmetry that structurally relates the first and second halves of the polypeptide chain to each other. Each half contains an antiparallel β-pleated sheet flanked by two helical segments and a C-terminal loop. Both domains contribute conserved residues to the metalloactive site. In each structure, a bis(μ-carboxylato)(μ-aqua/hydroxo)dicobalt core is observed, with an additional carboxylate residue at each metal site and a single histidine bound to cobalt 1 (Co1). Based on activity measurements, all of these enzymes have been proposed to be Co(II)-dependent enzymes.16,19 However, it has been shown that the addition of either Co(II), Fe(II), or Mn(II) provides enzymes that are catalytically competent.[20] More recently, *Ec*MetAP-I was shown to exhibit maximum catalytic activity with only one equivalent of either Co(II) or Fe(II).[20] The catalytically competent metal ion, assigned to M1, is ligated by His171 according to ^{1}H NMR and EXAFS data.[20,21] Based on these data, it was suggested that either Fe(II) or Mn(II) is the physiologically relevant metal ion and that all MetAPs function as a mononuclear metallohydrolase in vivo.[22,23] Interestingly, *Ec*MetAP-I can bind up to two equivalents of Mn(II), providing an enzyme that exhibits ~20% of the activity observed with Co(II)[24,25] and a team at Abbott Laboratories recently suggested that the physiologically relevant metal ion for *Hs*MetAP-II is Mn(II).[23]

Type-II MetAPs have been shown to be the target for the sesquiterpene epoxide-containing anti-angiogenesis agents ovalicin, fumagilin, and TNP-470, the last of which is currently in phase III clinical trials.[13,17,26,27,28] Type-I MetAPs have also been shown to covalently bind fumagilin through an active-site histidine residue which is identical to type-II MetAPs, albeit more slowly.[28] A significant aspect of designing small molecules that specifically target MetAPs is to gain a detailed understanding of how fumagillin, a covalently linked inhibitor, interacts with MetAPs. The X-ray crystal structure *Hs*MetAP-II complexed with fumagillin indicated that fumagillin covalently binds to an active-site histidine residue.[17] In addition, it was suggested that an alkoxide moiety on fumagillin, that resides 3.28 Å from an active-site metal ion, binds to the dinuclear active site. Herein, we demonstrate that Mn(II)-loaded *Ec*MetAP-I forms a bona fide dinuclear Mn(II) site. We also provide evidence that the mode of binding of fumagillin to *Ec*MetAP-I is analogous to that in *Hs*MetAP-II except that the alkoxide moiety on fumagillin is not an active-site ligand.

Materials and methods

Protein expression and purification

All chemicals used in this study were purchased commercially and were of the highest quality available. Recombinant wild-type *Ec*MetAP-I was expressed and purified as previously described.[20,25] Purified *Ec*MetAP-I exhibited a single band on SDS-PAGE and a single symmetrical peak in matrix-assisted laser desorption ionization time-of-flight (MALDI-TOF) spectrometric analysis, indicating M_r=29,630±10. Protein concentrations were estimated from the absorbance at 280 nm using an extinction coefficient of 16,450 M^{-1} cm^{-1}. Apo-*Ec*MetAP-I samples were exchanged into 25 mM Hepes (pH 7.5) containing 150 mM KCl (Centricon-10, Millipore). The protein was washed free of methionine using Chelex-treated methionine-free buffer (25 mM Hepes, pH 7.5, 150 mM KCl) prior to all kinetic assays. Samples of apo-*Ec*MetAP-I were routinely concentrated by microfiltration using a Microcon-10 concentrator (Amicon, Beverly, Mass., USA) and individual aliquots were stored in liquid nitrogen until needed.

Enzymatic assay

*Ec*MetAP-I was assayed for catalytic activity with the tetrapeptide MGMM as the substrate (8 mM) using an HPLC method as previously described.[20] This method is based on the spectrophotometric quantitation of the reaction product GMM following separation on a C8 HPLC column (Phenomenex, Luna; 5µ, 4.6×25 cm). The kinetic parameter *v* (velocity) was determined at pH 7.5 by quantifying the tripeptide GMM at 215 nm in triplicate. One unit of activity is defined as the amount of enzyme that produces 1 µmol of GMM in 1 min. The hydrolysis of MP-*p*-NA was monitored spectrophotometrically at 405 nm, based on the increase in absorbance of *p*-NA ($\Delta\varepsilon_{405}$ value of *p*-nitroaniline of 10,600 M^{-1} cm^{-1}) using a coupled assay.[29] The reaction mixture consisted of a 5-µL aliquot of a 10-µM enzyme solution, 3 µL of 2.0 mM prolidase in 20 mM Tris containing 30% glycerol. Various concentrations of substrate were added to the enzyme solution to a final volume of 1000 µL (25 mM Hepes in Chelexed water at pH 7.5 containing 150 mM KCl). Enzyme activities are expressed as units/mg, where one unit is defined as the amount of enzyme that releases 1 µmol of product at 30 °C in 1 min. Catalytic activities were determined with an error of ±10%.

Fumagillin-bound forms of [MnMn(*Ec*MetAP-I)]

Samples of [MnMn(*Ec*MetAP-I)]+fumagillin were prepared by the method of Lowther et al. [28]. Briefly, a 2.5 mM [MnMn(*Ec*MetAP-I)] sample in 25 mM Bicine buffer (pH 7.5) and 150 mM KCl was reacted with 10 equiv of fumagillin (Sigma, dissolved in dimethyl sulfoxide) under anaerobic conditions and frozen. [MnMn(*Ec*MetAP-I)]-fumagillin EPR samples were analyzed by MALDI on a linear time-of-flight mass spectrometer (TOF-MS) equipped with delayed ion extraction.[30,31] An ion source bias voltage of 24 kV and an extraction delay time of 1050 ns were employed. Ion extraction pulse voltages were selected to optimize mass resolution (via time lag focusing) for the largest *m*/*z* ion of interest in each sample. The ion signals generated from 100 individual laser shots (337 nm) were signal averaged to generate the resulting MALDI spectra. MALDI spectra were externally mass calibrated by the use of the flight times and known masses of the singly and doubly protonated ions produced by MALDI from a sample of*Ec*MetAP-I. [MnMn(*Ec*MetAP-I)]-fumagillin samples in Bicine buffer (pH 7.5) and 150 mM KCl were initially run down a C4 ZipTip (Millipore, Bedford, Mass., USA) prior to MALDI analysis to remove excess buffer and salts. The ZipTip was first treated with 30 µL of a 75% acetonitrile/25% distilled, deionized (DDI) water solution followed by 40 µL of a 0.1% trifluoroacetic acid (TFA) in DDI water solution. The [MnMn(*Ec*MetAP-I)]-fumagillin sample utilized for EPR analysis was diluted 20:1 with DDI water. Four successive 10-µL aliquots of the diluted protein sample were aspirated over the C4 modified silica packing of the ZipTip using a micropipette in order to bind proteins in the sample to the modified silica surface. Subsequent to binding, the ZipTip was washed with five successive 10-µL aliquots of 0.1% TFA in DDI water solution to remove the Bicine buffer and any other contaminating salts. The bound proteins were released from the ZipTip utilizing a 25 mM solution of 4-hydroxy-α-phenylcinnamic acid (Aldrich, Milwaukee, Wis., USA) prepared in 75% acetonitrile/25% DDI water with 0.1% TFA. A single 6-µL volume of the 4-hydroxy-α-phenylcinnamic acid was successively aspirated over the C4 modified silica packing of the ZipTip and 3 µL of this solution was deposited after the fourth aspiration onto the MALDI sample target and the solution allowed to evaporate. The non-volatile 4-hydroxy-α-phenylcinnamic acid served as the UV absorbing matrix for subsequent MALDI analysis.

Spectroscopic measurements

Low-temperature dual-mode EPR spectroscopy was carried out as in earlier work[32,33] using a Bruker ESP-300E spectrometer equipped with an ER 4116 DM dual-mode X-band cavity and an Oxford Instruments ESR-900 helium flow cryostat. EPR spectra were recorded at a modulation frequency of 100 kHz and at microwave frequencies of about 9.65 GHz and 9.37 GHz for perpendicular and parallel modes, respectively. Precise microwave frequencies were recorded for individual spectra to ensure precise *g*-alignment and all spectra and simulations are presented with respect to a magnetic field range corresponding to a microwave frequency of 9.646000 GHz. Other EPR recording parameters are specified in the figure legends.

Results

EPR spectroscopy of Mn(II)-substituted *Ec*MetAP-I

EPR spectra were recorded for *Ec*MetAP-I samples (~2.5 mM) to which one and two equivalents of Mn(II) were added (referred to as [MnMn(*Ec*MetAP-I)]). The spectra for each sample were indistinguishable except that the spectrum of [MnMn(*Ec*MetAP-I)] was twice as intense as that of *Ec*MetAP-I to which one equivalent of Mn(II) had been added.[34] Activity measurements showed a linear increase in activity with added Mn(II) up to 2.7±0.3 equiv.[24] An EPR spectrum recorded at 4 K on a 2.5-mM sample of [MnMn(*Ec*MetAP-I)] in Bicine buffer (pH 7.5) exhibited the characteristic six-line $g\approx2$ EPR signal of mononuclear Mn(II) (Fig. 1a). This signal was centered at $g=2.02$ (341 mT) and the $I=5/2$ hyperfine lines due to ^{55}Mn exhibited $A_{av}(^{55}Mn)=9.3$ mT (93 G). This is typical of Mn(II) in a ligand sphere composed of oxygen and/or nitrogen atoms.[35] That the signal is not due to uncomplexed Mn(II) can be clearly seen by comparison with the EPR signal observed at 4 K upon the addition of 5 mM $MnCl_2$ in Bicine buffer (pH 7.5) (Fig. 1c). Also evident in the spectrum of [MnMn(*Ec*MetAP-I)] is a six-line pattern centered at $g=4.15$ (166 mT) with $A_{av}(^{55}Mn)\approx9.0$ mT. This signal is often attributed to $\Delta m_s=2$ transitions that are formally forbidden for systems of high symmetry.[35,36,37] Other features in the spectrum include a weak six-line pattern centered at $g=9.0$ (77 mT) with $A_{av}(^{55}Mn)\approx9.0$ mT (part of which is shown magnified above Fig. 1a) and a signal extending out of zero field with poorly defined features that is again separated by ~9 mT. These features, in other systems, have been presumed to be due to inter-Kramer's doublet "fine structure" transitions where $m_s=\pm5/2\leftrightarrow\pm3/2$ and $m_s=\pm3/2\leftrightarrow\pm1/2$.[38] Thus, at 4 K, all of the spectral features can be attributed to a mononuclear Mn(II) species associated with *Ec*MetAP-I.

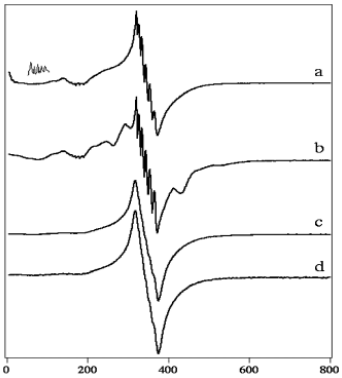

Fig. 1. EPR spectra of: (*a*) 2.5 mM [MnMn(*Ec*MetAP)] sample at 4 K, (*b*) 2.5 mM [MnMn(*Ec*MetAP)] sample at 41 K, (*c*) 5 mM $MnCl_2$ buffered solution at 4 K, and (*d*) 5 mM $MnCl_2$ buffered solution at 41 K. All samples were prepared in 25 mM Bicine buffer (pH 7.5) and 150 mM KCl. Spectra were recorded using 2.0 mW (*a*, *b*) or 5.0 mW (*c*, *d*)

microwave power and 0.8 mT modulation amplitude. The intensities of spectra *b*and *d* are shown comparative to *a* and *c*, respectively, after corrections for receiver gain differences and temperature. The *insert* above trace *a*, centered at 77 mT, is magnified 200 times

At higher temperatures, additional transitions were observed that cannot be accounted for by mononuclear Mn(II). An EPR spectrum of a 2.5 mM [MnMn(*Ec*MetAP-I)] sample recorded at 41 K (Fig. 1b) was found to clearly exhibit a number of transitions in addition to those observed at 4 K. The most intense of these additional transitions have resonance positions at g_{eff}=3.19 (216 mT), 2.85 (242 mT), 2.39 (289 mT), and 1.60 (430 mT). Weaker transitions are seen as a shoulder at g_{eff}=1.43 (482 mT), as a broad peak centered at g_{eff}=1.31 (526 mT), and as a broad absorption extending out of zero field. Additional structure observed in the *g*=2 region can occur because of forbidden transitions and *g* anisotropy due to a lower symmetry environment for Mn(II) when bound as monomeric Mn(II) in either a dinuclear active site or bound to the protein in a third, distinct or adventitious site. Since quantitation of these signals is difficult, at this time we were unable to accurately quantitate the amount of Mn(II) in the sample that accounts for these high-temperature signals. The appearance of these features at high temperature, and at unusual g_{eff} values, suggests that these signals are due to an excited state transition(s) in the *S*=1, 2 ... 5 non-Kramer's doublets due to two antiferromagnetically coupled Mn(II) ions with an *S*=0 ground state.[39,40] Closer inspection of the feature at *g*≈2.39 provided further evidence for the signals being due to a dinuclear species. Figure 2 shows the spectrum of a 2.5 mM [MnMn(*Ec*MetAP-I)] sample recorded at 41 K between 250 and 450 mT. Multiline hyperfine structure with a splitting of 4.4 mT can clearly be seen on the feature atg_{eff}=2.39 (289 mT), extending from 260 to 310 mT. These splittings are characteristic of exchange-coupled Mn(II) ions[35] and are a good indication that the additional features seen at 41 K are due to non-Kramer's doublet excited-state transitions due to spin-coupled Mn(II) ions.

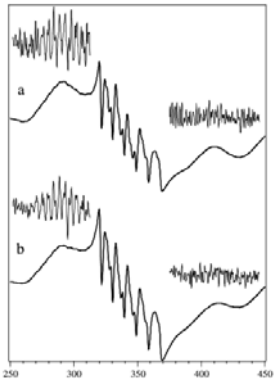

Fig. 2. EPR spectra of Mn(II)-loaded *Ec*MetAP-I in 25 mM Bicine buffer (pH 7.5) and 150 mM KCl at 41 K: 250–440 mT region of *Ec*MetAP-I with (*a*) one equivalent of Mn(II) and (*b*) two equivalents of Mn(II) added. Fourier filtering of the spectrum provides the traces above *a* and *b*. These data have been magnified 20 times, highlighting the 4.4-mT-split multiline signals

Final confirmation that the unusual signals seen at high temperature are due to an integer spin system was sought using parallel-mode EPR spectroscopy. Parallel-mode spectra recorded on [MnMn(*Ec*MetAP-I)] are presented in Fig. 3. At 4 K (Fig. 3a), the signal is dominated by an intense absorption emerging out of zero field and the transition is similar in appearance to that seen in the perpendicular mode. Both the perpendicular and parallel mode features exhibit a temperature dependence that follows Curie's law at low temperature but the signals decay rapidly at high temperature (parallel mode spectra are shown

recorded at 4, 10, 41, and 70 K in Fig. 3a–d, respectively). The g_{eff} value is also large for an integer-spin system, since one would expect $g_{eff}\approx 4S$. Thus, the most likely origin of this signal is one or more inter-Kramer's doublet fine structure transitions in mononuclear Mn(II). The spectrum also contains an intense trough-shaped feature with a minimum at g_{eff}=4.2 (165 mT), suggestive of an S=1 non-Kramer's doublet transition. The other two features in the spectrum at 4 K are two six-line patterns with average splittings of ~9.0 mT: the pattern at g=2.02 is presumably bleed-over of the intense perpendicular-mode signal, whereas the precise origin of the signal centered at$g\approx 4.8$ is unclear. Since both observed six-line patterns exhibit Curie-law temperature dependence as well as a 9-mT hyperfine splitting, they can be confidently assigned to mononuclear Mn(II).

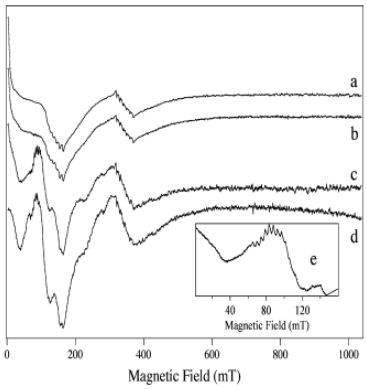

Fig. 3. Parallel-mode EPR spectra of [MnMn(*Ec*MetAP-I)] in 25 mM Bicine buffer (pH 7.5) and 150 mM KCl recorded at (*a*) 4 K, (*b*) 10 K, (*c*) 41 K, and (*d*) 70 K. Trace (*e*) is a high-resolution scan recorded at 50 K. Spectra were recorded at 20 mW microwave power, with 0.8 mT (*a*–*d*) or 0.4 mT (*e*) magnetic field modulation

The parallel-mode spectra of [MnMn(*Ec*MetAP-I)] recorded at 41 K and 70 K are shown in Fig. 3c and Fig. 3d, respectively. The spectra differ considerably from those recorded at 4 and 10 K (Fig. 3a and Fig. 3b). At 41 K (Fig. 3c) the lowest field feature is significantly weaker than at 4 K and at 70 K it is not visible. The two six-line patterns, which were clearly visible at 4 and 10 K, are still present but the $g\approx 4.8$ six-line signal is now obscured by other features. This feature can be visualized by Fourier filtering or polynomial subtraction of higher resolution spectra and is evident as an apparent splitting of the minimum feature at g_{eff}=4.2 (165 mT) and as structure on the small feature at g_{eff}=5.5 (125 mT). A number of features assignable to integral spin systems are present in the 41 K spectrum. There is a minimum feature at g_{eff}=4.2 (165 mT) which is suggestive of S=1, a peak at g_{eff}=8.0 (85 mT) which suggests S=2, a shoulder at g_{eff}=12 (58 mT), and a broad feature extending out of zero field that exhibits a minimum atg_{eff}=18 that could arise from either S=4 or S=5 or both. A quantitative temperature dependence of most of the features was not attempted as the signals overlap extensively; however, examination of Fig. 3 provides some useful information. The expected relative contributions to the spectrum from the S=1, 2 ... i spin multiplets are shown graphically in Fig. 4 for a system with J=7.0 cm^{-1}. As is evident from Fig. 4, the relative contributions from the higher spin multiplets increase with temperature. The minimum in the parallel-mode EPR spectrum of [MnMn(*Ec*MetAP-I)] at g_{eff}=18 is weak at 41 K but is pronounced at 70 K. In contrast, the minimum feature at g_{eff}=4.2 diminishes in intensity upon raising the temperature to 71 K. Furthermore, this feature is the only one ascribable to an integral spin system in the 4 K spectrum. These observations are entirely consistent with the assignment of the g_{eff}=18 feature to either S=4 or 5, and to the assignment of the g_{eff}=4.2 feature to S=1. The shoulder in the 41 K spectrum at g_{eff}=12 (58 mT) is resolved into a peak at 70 K, consistent with the doubling of

intensity expected for an *S*=3 spin state. Thus the assignments of the features in this spectrum on the basis of their resonance positions are supported by their temperature dependences.

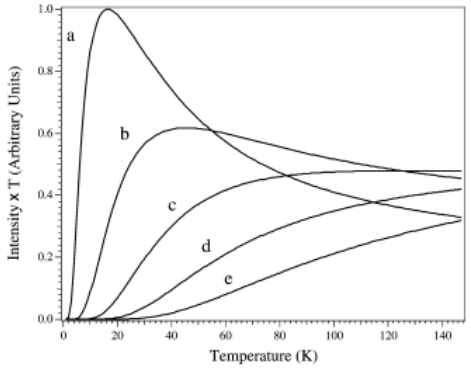

Fig. 4. Relative contributions to the parallel-mode EPR spectrum of [MnMn(*Ec*MetAP-I)] from the *S*=1, 2, 3, 4, 5 ... *i* spin multiplets (*a*–*e*) for a system with *J*=7.0 cm^{-1}

The most interesting feature observed in the parallel-mode EPR spectrum is a multiline signal centered about g_{eff}=8.0 (Fig. 3c), and the multiline signal can be clearly observed superimposed upon the broader features in the signal. The lines were split by ~4.5 mT, a hyperfine splitting similar to the multiline signal observed in the perpendicular-mode spectrum. A hyperfine pattern consisting of 11 lines separated by 4.5 mT and with intensity ratios of 1:2:3:4:5:7:5:4:3:2:1 would be indicative of two spin-coupled Mn(II) ions. However, because of the presence of the broader signals, the precise number of lines in the experimental spectrum and their relative intensities were difficult to estimate. Thus, it appears that the fine structure on the g_{eff}=8.0 feature is due to two exchange-coupled Mn(II) ions. This, in turn, suggests that the feature in the perpendicular-mode spectrum at g_{eff}=2.39 (289 mT; Fig. 2) that exhibits the 4.4 mT multiline splitting is also due to spin-coupled Mn(II) ions.

Each of the excited-state spin levels of a spin-coupled dinuclear Mn(II) system, *S*=1, 2, 3, 4, 5, can potentially exhibit features in the EPR spectrum. To obtain structural and electronic information about the small portion of spin-coupled Mn(II) ions in [MnMn(*Ec*MetAP-I)], the transitions responsible for at least some of the features in the EPR spectrum need to be identified. The features at g_{eff}=2.39 (289 mT) and 1.60 (430 mT) were chosen for study because they were the most intense and because the multiline pattern on the g_{eff}=2.39 signal was clear. Spectra were recorded over the temperature range 3.8–150 K and the *g*=2.02 six-line signal was eliminated by subtracting proportions of the 3.8 K signal, which exhibited no excited state features, from signals recorded at higher temperature. Thus, the temperature dependence of the g_{eff}=2.39 and g_{eff}=1.60 signals could be measured and the results are shown in Fig. 5. The temperature dependence of the *g*=2.02 six-line signal was also measured and clearly follows a 1/*T* Curie-law dependence (Fig. 5). In contrast, the g_{eff}=2.39 and g_{eff}=1.60 features exhibited a complex temperature dependence. For a spin ladder *S*=0, 1 ... *i*, the expected temperature-dependent weighted contribution to the EPR spectrum can be expressed by Eq. 1:

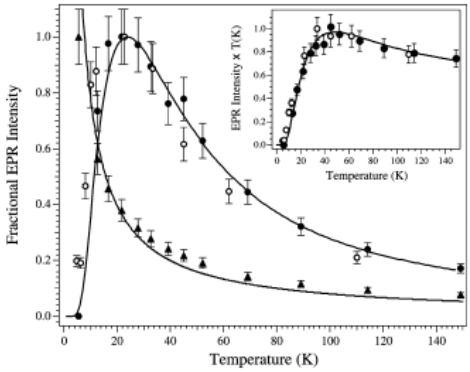

Fig. 5. EPR intensity versus temperature plot for $g\approx2$ signal (*triangles*) and for the resonances at 288 and 432 mT (*circles*). The *open* and *solid circles* represent data from two different samples. The *line* through the *triangles* is a fit to Curie behavior and the *line* through the*circles* is a fit to the Boltzmann distribution, assuming J=7.1 cm^{-1} and S=2. *Inset*: temperature-weighted data and fit

$$n_s(T) = \left\{(2S+1)\ exp\left[-\frac{S(S+1)J}{kT}\right]\right\} / \{\sum_I (2S_I +)\exp[-\frac{S(S_i+1)J}{kT}]\}$$

where $n_s(T)$ is the fractional population of the spin state S, S_i=0, 1, 2, 3, 4, 5, and J is the exchange coupling between the two Mn(II) ions. A graphic display of the consequences of this expression is given as Fig. 4. The data for both the g_{eff}=2.39 and g_{eff}=1.60 features of [MnMn(*Ec*MetAP-I)] were best simulated assuming a quintet S=2 spin state with $J\approx$7.0 cm^{-1}(Fig. 5). Attempts to fit the temperature dependence of the intensities of the g_{eff}=2.39 andg_{eff}=1.60 features to either an S=1 state or a mixed triplet-quintet population were entirely unsuccessful, whereas the fit to a pure S=2 state is clearly very good over a wide temperature range. Thus the contribution to the resonances at 289 and 430 mT from the triplet S=1 state must be very small. The positions of these quintet state resonances has been shown to be a function of the zero-field splitting of that state, D_2,[41] and in [MnMn(*Ec*MetAP-I)] these correspond to a D_2 value of −0.175 cm^{-1}. Because of the dipole–dipole component of D_2, it is very sensitive to the inter-manganese distance, and by comparison with model compound data[39] the inter-manganese distance in [MnMn(*Ec*MetAP-I)] was estimated to be 3.1 Å. This value is in very good agreement with the crystallographically determined cobalt–cobalt distance of 3.2 Å for [CoCo(*Ec*MetAP-I)].[15,42]

EPR spectroscopy of Mn(II)-substituted *Ec*MetAP-I in the presence of fumagillin

In order to determine how the anti-angiogenesis agent fumagillin interacts with the Mn(II)-active site of *Ec*MetAP-I, both MALDI-TOF mass spectrometry and EPR spectroscopy were used to investigate fumagillin binding. In the MALDI-TOF mass spectrum of [MnMn(*Ec*MetAP-I)] a symmetric peak was observed at M_r=29,335±10. On the other hand, the MALDI-TOF mass spectrum of [MnMn(*Ec*MetAP-I)]-fumagillin provided a second symmetric peak at M_r=29,786±10, which is 451 Da larger than that observed for the purified, native form of *Ec*MetAP-I. This change in mass is in good agreement with the mass of fumagillin, which is 458.6 Da, and indicates that fumagillin is covalently bound to [MnMn(*Ec*MetAP-I)]. The identical sample used in the mass spectrometry experiment was also used to record the EPR spectrum of [MnMn(*Ec*MetAP-I)]-fumagillin (Fig. 6b). The signal at $g\approx2$, which makes up the bulk of the Mn(II) in the sample, is identical to that of the uncomplexed Mn(II)-loaded enzyme. The most marked change in the EPR spectrum of [MnMn(*Ec*MetAP-I)]-fumagillin is a shift in the 4.5 mT

multiline signals by 2.0 mT in the region 260–315 mT (Fig. 7A). The resolution of the experiment is well within this value and also the position of the internal standard, provided by the sharp feature due to mononuclear Mn(II) at 321.8 mT, is identical in both spectra. Furthermore, measurement of the relative intensities of these multiline splittings reveals that the lines in the EPR spectrum of *Ec*MetAP-I treated with fumagillin are on average 30% more intense than those of untreated enzyme (Fig. 6). This implies a decrease in the *g*-strain of the Mn(II) centers in [MnMn(*Ec*MetAP-I)] upon fumagillin binding and, thus, a decrease in the vibrational freedom compared to the untreated [MnMn(*Ec*MetAP-I)]. A final difference is the observation of a weak but detectable multiline splitting pattern in the 387–434 mT region in the fumagillin-treated [MnMn(*Ec*MetAP-I)] enzyme (Fig. 7B). This pattern is not detectable in untreated [MnMn(*Ec*MetAP-I)] enzyme, presumably because of the line broadening due to the higher the *g*-strain. Thus the EPR data indicate that binding of fumagillin does not alter the mononuclear Mn(II) in the active site of *Ec*MetAP-I, and only slightly perturbs the spin coupling between the two Mn(II) ions in the minor signal due to dinuclear Mn(II) centers.

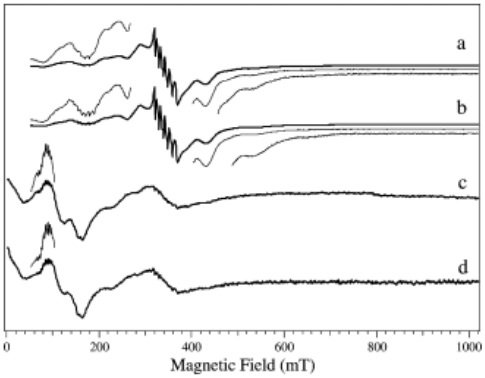

Fig. 6. EPR spectra of [MnMn(*Ec*MetAP-I)] in 25 mM Bicine buffer (pH 7.5) and 150 mM KCl at 41 K: (*a*) native enzyme and (*b*) in the presence of 10 equiv of fumagillin. Parallel-mode EPR spectra of [MnMn(*Ec*MetAP-I)] in 25 mM Bicine buffer (pH 7.5) and 150 mM KCl recorded at 41 K: (*c*) native enzyme and (*d*) in the presence of 10 equiv of fumagillin. The traces *above* or *below* the spectral traces have been magnified 20 or 40 times, respectively, highlighting the 4.4 mT-split multiline signals

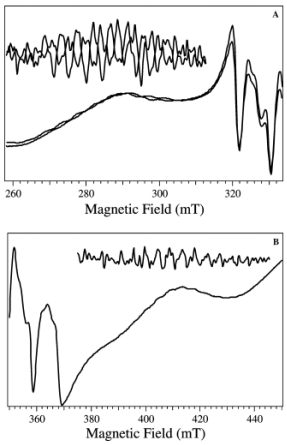

Fig. 7A, B. EPR spectra of [MnMn(*Ec*MetAP-I)] in 25 mM Bicine buffer (pH 7.5) and 150 mM KCl at 41 K. **A** 250–330 mT region where the *solid line* is [MnMn(*Ec*MetAP-I)] and the *dashed line* is [MnMn(*Ec*MetAP-I)]+fumagillin. The traces *above* the spectral traces have been magnified 200 times, highlighting the shift in the 4.4-mT-split multiline signals. **B** 350–450 mT region of [MnMn(*Ec*MetAP-I)]+fumagillin. The trace *above* the spectral trace has been magnified 200 times

Discussion

Amide bond hydrolysis is a common enzymological reaction and the same chemistry can be catalyzed by several different metalloenzymes, including aminopeptidases, carboxypeptidases, endopeptidases, β-lactamases, ureases, and penicillin amidases.[43] Many of these enzymes utilize Zn(II) ions in their catalytic active site; however, several have been shown to be partially active or even hyperactive with one or more first-row transition metal ions, ranging from Mn(II) to Zn(II). Whole-cell studies on *Ec*MetAP-I suggested that the in vivo metal ion for all MetAPs was either Fe(II) or Mn(II).[25] Recently, the physiologically relevant metal ion for*Hs*MetAP-II was assigned as Mn(II) using Mn(II)-specific synthetic inhibitors to probe intracellular *Hs*MetAP-II.[23] That Mn(II) can activate *Ec*MetAP-I[24] is not surprising since the Mn(II)-dependant aminopeptidase P from *E. coli* (AMPP) has active site ligands that are identical to those of MetAPs. Interestingly, AMPP has been suggested to be a Mn(II)-dependent enzyme.[44,45] In order to gain insight into the metal binding properties of *Ec*MetAP-I, we have recorded EPR spectra of the Mn(II)-loaded forms.

High-spin octahedral Mn(II) ions posses an ^{6}S electronic ground state that can be split by zero-field effects when Mn(II) is placed in a ligand field.[46] Zero-field splitting produces three Kramer's doublets (M_s=$\pm^1/_2$, $\pm^3/_2$, $\pm^5/_2$) whose degeneracy is removed in the presence of a magnetic field. The result of this splitting is five allowed (ΔM_s=±1) EPR transitions. Coupling of the ^{55}Mn nuclear spin (I=$^5/_2$) to the electronic spin further complicates the observed EPR spectra and results in a six-fold hyperfine splitting pattern that produces 30 possible allowed (ΔM_s=±1 and ΔM_I=0) transitions. Additional complications result from the outer fine-structure transitions ($\pm^5/_2 \rightarrow \pm^3/_2$ and $\pm^3/_2 \rightarrow \pm^1/_2$) that are not usually well resolved for highly anisotropic protein coordination environments. The most distinctive EPR signature for a high-spin Mn(II) center is the ($+^1/_2 \rightarrow -^1/_2$) fine-structure transition that is nearly isotropic and typically gives rise to an intense signal at g=2 with a resolved six-fold hyperfine splitting pattern. The magnetic spin levels of a Mn(II) ion can be described by the spin hamiltonian:

$$H = g\beta\mathbf{B}\cdot\mathbf{S} + D\left(\mathbf{S}_z^2 - \frac{35}{12}\right) + E\left(\mathbf{S}_x^2 - \mathbf{S}_y^2\right) + \mathrm{A}\mathbf{SI}$$

where D and E have their usual meanings. It has been previously reported that significant changes in the nuclear hyperfine coupling constant, A, reflects covalency changes in metal–ligand interactions.[35,47] The X-band EPR spectrum of the Mn(II)-loaded *Ec*MetAP-I ([MnMn(*Ec*MetAP-I)]) at 4 and 41 K reveals a strong hyperfine split signal centered at g=2, characteristic of the ($+^1/_2 \rightarrow -^1/_2$) transition. As a control, the X-band EPR spectra of $[Mn(H_2O)_6]^{2+}$ in buffer were recorded and these data revealed that the observed signals are distinct from those obtained for [MnMn(*Ec*MetAP-I)] samples. The hyperfine coupling constant, A, measured directly from the spacing of the most intense signals about g=2.02, is ~9.5 mT. This is consistent with Mn(II) ions being coordinated by oxygen- and nitrogen-containing ligands.[35] The signal centered about g≈4.0 with resolvable ^{55}Mn hyperfine splitting (A=95 G) definitively assigns it to the Mn(II) ions in *Ec*MetAP-I and not an Fe(III) impurity. Similar signals have been previously observed for very anisotropic Mn(II) centers in proteins and were assigned to a ΔM_s=±2 transition.[35]

The EPR spectrum of Mn(II)-loaded *Ec*MetAP-I suggests that some proportion of the Mn(II) in*Ec*MetAP-I is mononuclear. However, multiple lines of evidence from the EPR data exist for a significant population of dinuclear Mn(II) in *Ec*MetAP-I; the similarity of resonance positions to inorganic exchange-coupled Mn(II) species, their temperature dependences, the parallel mode data, and the resolved 4.5 mT multiline hyperfine pattern all indicate dinuclear Mn(II). Recently it was reported that *Ec*MetAP-I

contains a high- and a low-affinity metal binding site for Fe(II) and Mn(II) and that these enzymes are maximally active when only one metal binding site is occupied.[24,25] On the basis of the similarity of the EPR signals of *Ec*MetAP-I with both one and two equivalents of Mn(II), it seems likely that there exists both a dinuclear Mn(II) and a mononuclear Mn(II) associated with *Ec*MetAP-I, at least at the high concentrations used for spectroscopy and crystallography. Since X-ray crystallographic data suggest a dinuclear active site can form in *Ec*MetAP-I, the EPR-detected dinuclear center almost certainly constitutes the active site. Activity and EPR measurements suggest that the dinuclear site is formed by the cooperative binding of two Mn(II) ions, and the EPR signal due to mononuclear Mn is clearly distinct from that of Mn(II) in buffer. It is, therefore, more likely that the mononuclear species is a distinct Mn(II) ion associated with the protein rather than an Mn-depleted active site.

An important class of MetAP inhibitor based on natural products of fungal origin comprise fumagillin, ovalicin, and TNP-470. Ovalicin and a synthetic analog of fumagillin (TNP-470) have been shown to preferentially inhibit endothelial cell growth in tumor vasculature in vivo.[48] Based on fumagillin-specific affinity reagents and mass spectrometric studies on MetAP-fumagillin complexes, MetAPs were identified as the specific target of fumagillins.[26,49] The mode of inhibition was shown to be via the formation of a covalent bond between a conserved histidine residue in MetAPs and an epoxide carbon moiety on fumagillin.[26,28,49,50] Confirmation that fumagillin reacts with *Ec*MetAP-I comes from mass spectrometric and N-terminal sequence analysis, which indicated that fumagillin covalently binds to an active-site histidine residue (His79) that is not a ligand at the dinuclear active-site cluster.[28] In order to gain structural information on the interaction between the Mn(II) active site of *Ec*MetAP-I and the anti-angiogenesis drug fumagillin, X-band EPR spectra of [MnMn(*Ec*MetAP-I)] were recorded after reaction with fumagillin. That fumagillin was covalently bound to the Mn(II)-loaded *Ec*MetAP-I enzyme was verified by MALDI-TOF spectrometric analysis of the EPR samples, which revealed a mass shift of 451 Da, in excellent agreement with the mass of fumagillin (458 Da). Interestingly, and perhaps surprisingly, no significant change in the X-band EPR spectra recorded in either the perpendicular or parallel modes were observed, except for a 2.5 mT change in the position of the 4.5 mT multiline signals observed on the $g \approx 2.39$ signal. These data strongly suggest that upon fumagillin binding, no protein-derived ligand atoms or metal-bound water molecules are displaced. In addition, the single oxygen atom bridge between the minor dinuclear species is not displaced since this would have likely resulted in a change in the Mn–Mn distance that would be expected to result in a perturbation of the Heisenberg exchange interaction. Moreover, these data are also inconsistent with the replacement of the bridging water molecule with a bridging alkoxide atom from fumagillin, since such a change would clearly alter the Heisenberg exchange interaction.

Combination of the EPR spectroscopic results for the fumagillin-bound [MnMn(*Ec*MetAP-I)] with the recent X-ray crystal structure of the type-II MetAP from *H. sapiens* complexed with fumagillin, at 1.8 Å resolution, reveals some interesting similarities and differences. The epoxide-bearing side chain of fumagillin occupies the putative substrate-binding pocket of*Hs*MetAP-II. The long unsaturated side-chain is analogous to the COOH-terminal peptide chain in the X-ray structure of a substrate analog inhibited form of *Ec*MetAP-I.[15,42] The crystallographic results also verify that a covalent bond is formed between the reactive ring epoxide of fumagillin and His231 in the active site of the type-II MetAP. The oxygen atom liberated from the breaking of the epoxide bond is 3.28 Å away from Co1, the Co(II) ion bound by His331, Glu364, and the two bridging carboxylate residues Asp262 and Glu459. This alkoxide oxygen atom was suggested to be directly coordinated to Co1. The EPR results presented herein clearly indicate

that the alkoxide oxygen atom of fumagillin is *not* coordinated to either the mononuclear Mn(II) center in the active site of *Ec*MetAP-I or the dinuclear component, contrary to that suggested by Liu et al.[17] Closer inspection of the X-ray crystal structure of *Hs*MetAP-II complexed by fumagillin indicates that the approximate location of the alkoxide oxygen of fumagillin is where a water molecule resided at >3 Å from the Co(II) ion in the uncomplexed structure. Therefore, we propose that the oxygen atom liberated upon the addition of fumagillin to *Ec*MetAP-I displaces the water molecule that bridges between His178 and the water molecule bridging between the two Co(II) ions as revealed in the X-ray structure of native *Ec*MetAP-I (Fig. 8). This structure is also consistent with EXAFS data reported for the Co(II)-loaded form of *Ec*MetAP-I in the presence of fumagillin.[21] Thus, fumagillin does *not*provide a ligand to either metal ion in the dinuclear active site, nor does it bridge between the two metal ions, but instead slightly perturbs the Mn(II) centers through a H-bonding interaction with a bound water molecule. Since fumagillin has two reactive epoxide moieties, it is quite cytotoxic, probably due to alkylation of other biomolecules within the cell. Therefore, understanding the molecular mechanism of the MetAP-catalyzed cleavage of N-terminal methionine residues, as well as the binding mode of known anti-angiogenesis drugs, will facilitate the rational design of new, more potent MetAP inhibitors with improved in vivo stability, specificity, and lower cytotoxicity.

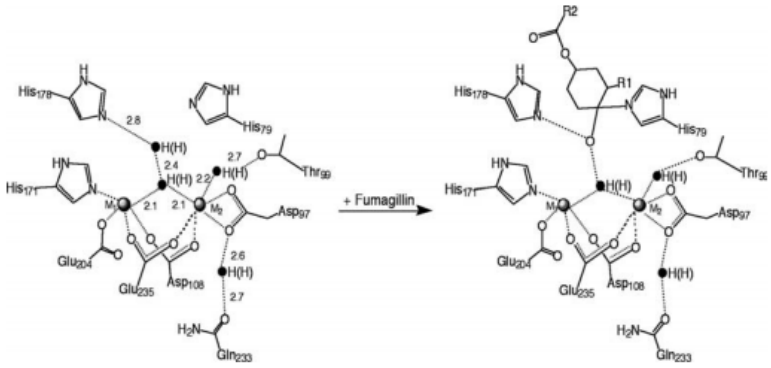

Fig. 8. Proposed binding scheme for fumagillin to the active site of *Ec*MetAP-I

Notes

Acknowledgements

This work was supported by the National Institutes of Health (GM-56495 to R.C.H. and AI-056231 to B.B.) and the National Science Foundation (CHE-0240810 to R.C.H.). The Bruker ESP-300E EPR and ARX-400 NMR spectrometers were purchased with funds provided by the National Science Foundation (BIR-9413530 and CHE-9311730, respectively) and Utah State University. The methionyl aminopeptidase from *E. coli* was purified from a stock culture kindly provided by Drs Brian Matthews and W. Todd Lowther. The program EPRSim XOP was made available by Dr John Boswell, Oregon Graduate Institute.

References

1. Bradshaw RA (1989) Trends Biochem Sci 14:276–279
2. Meinnel T, Mechulam Y, Blanquet S (1993) Biochimie 75:1061–1075
3. Bradshaw RA, Brickey WW, Walker KW (1998) Trends Biochem Sci 23:263–267
4. Arfin SM, Bradshaw RA (1988) Biochemistry 27:7979–7984
5. Tobias JW, Shrader TE, Rocap G, Varshavsky A (1991) Science 254:1374–1377

6. Arfin SM, Kendall RL, Hall L, Weaver LH, Stewart AE, Matthews BW, Bradshaw RA (1995) Proc Natl Acad Sci USA 92:7714–7718
7. Bachmair A, Finley D, Varshavsky A (1986) Science 234:179–234
8. Rajagopalan PTR, Datta A, Pei D (1997) Biochemistry 36:13910–13918
9. Chang S-YP, McGary EC, Chang S (1989) J Bacteriol 171:4071–4072
10. Chang Y-H, Teichert U, Smith JA (1992) J Biol Chem 267:8007–8011
11. Li X, Chang Y-H (1995) Proc Natl Acad Sci USA 92:12357–12361
12. Miller CG, Kukral AM, Miller JL, Movva NR (1989) J Bacteriol 171:5215–521
13. Kruger EA, Figg WD (2000) Expert Opin Invest Drugs 9:1383–1395
14. Tahirov TH, Oki H, Tsukihara T, Ogasahara K, Yutani K, Ogata K, Izu Y, Tsunasawa S, Kato I (1998) J Mol Biol 284:101–124
15. Lowther WT, Orville AM, Madden DT, Lim S, Rich DH, Matthews BW (1999) Biochemistry 38:7678–7688
16. Roderick LS, Matthews BW (1993) Biochemistry 32:3907–3912
17. Liu S, Widom J, Kemp CW, Crews CM, Clardy J (1998) Science 282:1324–1327
18. Oefner C, Douangamath A, D'Arcy A, Hafeli S, Mareque D, MacSweeney A, Padilla J, Pierau S, Schulz H, Thormann M, Wadman S, Dale GE (2003) J Mol Biol 332:13–21
19. Tahirov TH, Oki H, Tsukihara T, Ogasahara K, Izu Y, Tsunasawa S, Kato I, Yutani K (1997) Acta Crystallogr Sect D 53:798–801
20. D'souza VM, Bennett B, Copik AJ, Holz RC (2000) Biochemistry 39:3817–3826
21. Cosper NJ, D'souza V, Scott R, Holz RC (2001) Biochemistry 40:13302–13309
22. Meng L, Ruebush S, D'souza VM, Copik AJ, Tsunasawa S, Holz RC (2002) Biochemistry 41:7199–7208
23. Wang J, Sheppard GS, Lou P, Kawai M, Park C, Egan DA, Schneider A, Bouska J, Lesniewski R, Henkin J (2003) Biochemistry 42:5035–5042
24. D'souza VM, Swierczek SI, Cosper NJ, Meng L, Ruebush S, Copik AJ, Scott RA, Holz RC (2002) Biochemistry 41:13096–13105
25. D'souza VM, Holz RC (1999) Biochemistry 38:11079–11085
26. Griffith EC, Su Z, Turk BE, Chen S, Chang Y-H, Wu Z, Biemann K, Liu JO (1997) Chem Biol 4:461–471
27. Sin N, Meng L, Wang MQW, Wen JJ, Bornmann WG, Crews CM (1997) Proc Natl Acad Sci USA 94:6099–6103
28. Lowther WT, McMillen DA, Orville AM, Matthews BW (1998) Proc Natl Acad Sci USA 95:12153–12157
29. Zhou Y, Gou X-C, Yi T, Yoshimoto T, Pei D (2000) Anal Biochem 280:159–165
30. Brown RS, Lennon JJ (1995) Anal Chem 67:1998
31. Brown RS, Lennon JJ (1995) Anal Chem 67:3990
32. Bennett B, Holz RC (1997) J Am Chem Soc 119:1923–1933
33. Bennett B, Holz RC (1997) Biochemistry 36:9837–9846
34. Copik AJ, Nocek B, Swierczek SI, Ruebush S, SeBok J, D'souza VM, Peters J, Bennett B, Holz RC (2004) Biochemistry 43:(in press)
35. Reed GH, Markham GD (1984) Biol Magn Reson 6:73–142
36. Griscom DL, Griscom RE (1967) J Chem Phys 47:2711–2722
37. Schreurs JWH (1978) J Chem Phys 69:2151–2156
38. Rusnak F, Yu L, Todorovic S, Mertz P (1999) Biochemistry 38:6943–6952
39. Khangulov SV, Pessiki PJ, Barynin VV, Ash DE, Dismukes GC (1995) Biochemistry 34:2015–2025

40. Khangulov SV, Sossong TMJ, Ash DE, Dismukes GC (1998) Biochemistry 37:8539–8550
41. Baranowski J, Cukierda T, Jezowska-Trzebiatowska B, Kozlowski H (1979) J Magn Reson 33:585–593
42. Lowther TW, Zhang Y, Sampson PB, Honek JF, Matthews BW (1999) Biochemistry 38:14810–14819
43. Wilcox DE (1996) Chem Rev 96:2435–2458
44. Wilce MCJ, Bond CS, Dixon NE, Freeman HC, Guss JM, Lilley PE, Wilce JA (1998) Proc Natl Acd Sci USA 95:3472–3477
45. Zhang L, Crossley MJ, E. DN, Ellis PJ, Fisher ML, King GF, Lilley PE, MacLachlan D, Pace RJ, Freeman HC (1998) J Biol Inorg Chem 3:470–483
46. Drago RS (1992) Physical methods for chemists, 2nd edn. Saunders, Orlando, Fla., USA
47. Whiting AK, Boldt YR, Hendrich MP, Wackett LP, Que L (1996) Biochemistry 35:160–170
48. Yamamoto T, Sudo K, Fujita T (1994) Anticancer Res 14:XXX–XXX
49. Sin N, Meng L, Wang MQ, Wen JJ, Bornmann WG, Crews CM (1997) Proc Natl Acad Sci USA 94:6099–6103
50. Turk BE, Su Z, Liu JO (1998) Bioorg Med Chem 6:1163–1169